Physica E 44 (2011) 12–16

Contents lists available at ScienceDirect

Physica E

journal homepage: www.elsevier.com/locate/physe

Elastic instability of bilayer graphene using atomistic finite element

Y. Chandra [a], R. Chowdhury [a,*], S. Adhikari [a], F. Scarpa [b]

[a] Multidisciplinary Nanotechnology Centre, Swansea University, Swansea SA2 8PP, UK
[b] Advanced Composites Centre for Innovation and Science, University of Bristol, Bristol BS8 1TR, UK

ARTICLE INFO

Article history:
Received 20 April 2011
Accepted 16 June 2011
Available online 23 July 2011

ABSTRACT

In-plane elastic instability of bilayer graphene sheets is investigated using atomistic finite element approaches. The equivalent homogenised properties of graphene sheet are expressed in terms of the thickness, equilibrium lengths and force-field models used to represent the C–C bonds of the graphene lattice. The covalent bonds are represented as structural beams with stretching, bending, torsional and shear deformation, and the strain energies associated to affine deformation mechanisms. The overall mechanical properties and geometric configurations of the nano-structures represented as truss assemblies are then calculated minimising the total potential energy associated to the loading, thickness and average equilibrium lengths of the bonds. Different boundary conditions and aspect ratios are considered for both bilayer and single-layer graphene sheets. The bilayer graphene sheets are found to be offering remarkably higher buckling strengths as compared to single-layer sheets.

1. Introduction

Graphene has attracted tremendous attention in both its 2D and 1D forms, since the discovery of superlattice monolayers and thin films of graphite [1,2]. In an experimental work in 2004, Meyer et al. [3] were the first to report the possibility of suspending single-layer graphene sheets (SLGSs) [4] in vacuum, e.g., the possibility of bilayer graphene sheets (BLGSs). BLGSs are two atom thick array of carbon sp^2 bonds forming a double layer SLGS, with an interlayer spacing of 0.34 nm [5]. Pal and Ghosh [6,7] have investigated the low-frequency electrical resistance fluctuations in bilayer and multilayer graphene. BLGSs offer unique and excellent electrical properties making them very suitable candidate for next generation semiconductors [8,9]. Significant studies [5,10–16] exist on the stiffness of single and multilayer graphene sheets by considering static deformations and natural frequencies. However, very few literature [17,18] exists in the area of elastic instabilities of graphene sheets using nonlocal continuum mechanics. In the present work, we have performed eigenvalue buckling analysis on both SLGSs and BLGS structures. The extraction of buckling modes by eigenvalue scheme is viable in this case, since the objective of this paper is to compute critical buckling loads. However it is a common practice to perform nonlinear buckling analysis on carbon nanotubes [19–21], since the simulation of local buckling mode shapes was the key objective of these research papers.

The authors have recently formulated a modelling approach, where the equivalent homogenised properties of a graphene sheet are expressed in terms of the thickness, equilibrium lengths and force-field models used to represent the C–C bonds of the graphene lattice [22]. The covalent bonds are represented as structural beams with stretching, bending, torsional and deep shear deformation, based on the equivalence between the harmonic potential expressed in terms of Morse and Amber models [23], and the strain energies associated to affine deformation mechanisms. The overall mechanical properties and geometric configurations of the nanostructures represented as truss assemblies (finite elements) are then calculated minimising the total potential energy associated to the loading, thickness and average equilibrium lengths of the bonds. A typical example of a BLGS is shown in Fig. 1. Various possible scenarios, namely different boundary conditions and aspect ratio are considered in the present study. The layout of the paper is as follows. In the next section, we present the atomistic approach utilised in the present analysis. This discussion will include mathematical behavior of C–C covalent bonds and interlayer Lennard-Jones (L-J) potential. The results of the analysis will be presented in the fourth section. The results will elucidate dependence of buckling response on aspect ratio, boundary conditions and number of layers. Finally, the paper will be completed by concluding remarks on the present study.

2. Atomistic finite element approach

2.1. Modelling of carbon–carbon covalent bonds

The carbon–carbon sp^2 are modelled as Timoshenko beams with axial, out-of-plane and in-plane rotational degrees of freedom.

* Corresponding author. Tel.: +44 1792 602969; fax: +44 1792 295676.
E-mail address: R.Chowdhury@swansea.ac.uk (R. Chowdhury).

1386-9477/$ - see front matter © 2011 Elsevier B.V. All rights reserved.
doi:10.1016/j.physe.2011.06.020

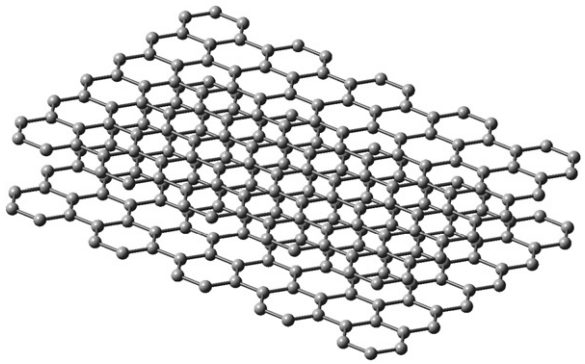

Fig. 1. Bilayer graphene sheet: atomic configuration of width = 19.074 Å and length = 19.538 Å.

The harmonic potential of the C–C bond is given as [24–26]

$$U_r = \tfrac{1}{2}k_r(\delta r)^2, \quad U_\theta = \tfrac{1}{2}k_\theta(\delta\theta)^2, \quad U_\tau = \tfrac{1}{2}k_\tau(\delta\varphi)^2 \tag{1}$$

The equivalent mechanical properties of the C–C bond can be calculated using a beam mapping technique, imposing the equivalence between the harmonic potential and the mechanical strain energies of a hypothetical structural beam of length L [22]:

$$\frac{k_r}{2}(\delta r)^2 = \frac{EA}{2L}(\delta r)^2 \tag{2a}$$

$$\frac{k_\tau}{2}(\delta\varphi)^2 = \frac{GJ}{2L}(\delta\varphi)^2 \tag{2b}$$

$$\frac{k_\theta}{2}(\delta\theta)^2 = \frac{EI}{2L}\frac{4+\Phi}{1+\Phi}(\delta\theta)^2 \tag{2c}$$

Eq. (2a) represents stretching and axial deformation mechanism (with E being the equivalent Young's modulus), while Eq. (2b) represents the torsional deformation of the C–C bond with the pure shear deflection of the structural beam associated to an equivalent shear modulus G. Eq. (2c) accounts for the shear deformation in the cross section. For circular cross sections, the shear deformation constant can be expressed as [22]

$$\Phi = \frac{12EI}{GA_sL^2} \tag{3}$$

In Eq. (3), $A_s = A/F_s$ is the reduced cross section of the beam by the shear correction term F_s [27]:

$$F_s = \frac{6+12\nu+6\nu^2}{7+12\nu+4\nu^2} \tag{4}$$

The insertion of Eqs. (3) and (4) in Eq. (2) leads to a nonlinear relation between the thickness d and Poisson's ratio ν of the equivalent beam [22]:

$$k_\theta = \frac{k_r d^2}{16}\frac{4A+B}{A+B} \tag{5}$$

where

$$A = 112L^2k_\tau + 192L^2k_\tau\nu + 64L^2k_\tau\nu^2 \tag{6}$$

$$B = 9k_rd^2 + 18k_rd^4\nu + 9k_rd^4\nu^2 \tag{7}$$

The values of the Morse force constants are $k_r = 8.74\times10^{-7}$ N mm^{-1}, $k_\theta = 9.00\times10^{-10}$ N nm rad^{-2} and $k_\tau = 2.78\times10^{-10}$ N nm^{-1} rad^{-2}. The equivalent mechanical properties of the C–C bond can be calculated by performing a nonlinear optimisation of Eqs. (2a)–(2c) using a Marquardt algorithm [28]. The C–C bond can then be discretised as a single two-node 3D FE model beam with a stiffness matrix described in Ref. [29], where the nodes represent the atoms. For comprehensive understanding of the above procedure, readers are referred to Refs. [12,22].

2.2. Modelling the interlayer potential

The equivalent axial force due to the L-J potential between the pair of atoms (i, j) belonging to different graphite layers can be expressed as [12]

$$F_{ij} = \frac{\partial V_{ij}}{\partial r} \tag{8}$$

where r is the atomic displacement along **ij** (layer–layer length). According to Girifalco et al. [30], the force between the atoms (ij) can also be represented by

$$F_{ij} = -12\varepsilon\left[\left(\frac{r_{min}}{y}\right)^{13} - \left(\frac{r_{min}}{y}\right)^{7}\right] \tag{9}$$

where $y = r_{min} + \delta r$, δr is the atomic displacement along the length **ij**. The r_{min} (in Å) is given by $2^{1/6}\sigma$, where $\sigma = (A/B)^{1/6}$. The B and A are attractive and repulsive constants, and for our cases of boundary conditions, they are given by 24.3×10^3 eV Å^{12} and 15.4 eV Å^6 respectively, and ε is $B^2/(4A)$. In the atomistic models, we have used spring elements to form a nonlinear connection between two layers of the bilayer structure representing L-J potentials. The force deflection curve for L-J springs has been calculated by using the relation in Eq. (9).

3. Results and discussions

The eigenvalue analysis of bilayer graphene sheets depends on the boundary conditions. Thus, in this work, we analyze two groups of BLGS, i.e., cantilevered BLGS and bridged BLGS with varying aspect ratio. The cantilever (CFFF) and bridge models (CCFF) are depicted in Figs. 2(a) and 3(a) respectively. Buckling analysis has been carried out using the atomistic finite element approach, consisting in creating a geometric stiffness matrix imposing first a unit force along the buckling direction, and then computing the eigenvalues and related eigenmodes with a Lanczos solver. The BLGS buckling mode shapes at CFFF and CCFF conditions are depicted in Figs. 2(b) and 3(b) respectively. These buckling mode shapes for BLGS are found to be identical to those of SLGS (figure not shown).

3.1. Dependence of SLGS and BLGS buckling loads on length and aspect ratio

The variation of SLGS critical buckling load with length is shown in Fig. 4. Fig. 5 presents the variation of BLGS buckling with length. The value of critical buckling load at a given length is found to be independent of aspect ratio, and decreases with increase in length. This variation of buckling strength with the side length is also inline with those of elastic plates presented in the classical literature [31,32]. For bridged SLGS with length raising from 2 to 20 nm, the critical buckling load is found to be decreased in the range of about 6–1 N. For bridged BLGS, this range is found to be about 180–80 N. This indicates that, at a given length and under buckling loads, the BLGS is stronger than SLGS by a factor of more than 30. The pattern of variation of buckling loads for BLGS is found to be dissimilar to that of SLGS. This dissimilarity is primarily due to the presence of nonlinearity in the interlayer L-J potential.

3.2. Dependence of SLGS and BLGS buckling load on the boundary condition

Under the influence of buckling loads, the bridged plate structure generally offers higher stiffness [31,32] as compared to the cantilever structure. Referring to Fig. 4 and making a comparison between CCFF-SLGS and CFFF-SLGS models indicates that changing the boundary condition from one edge fixed to both

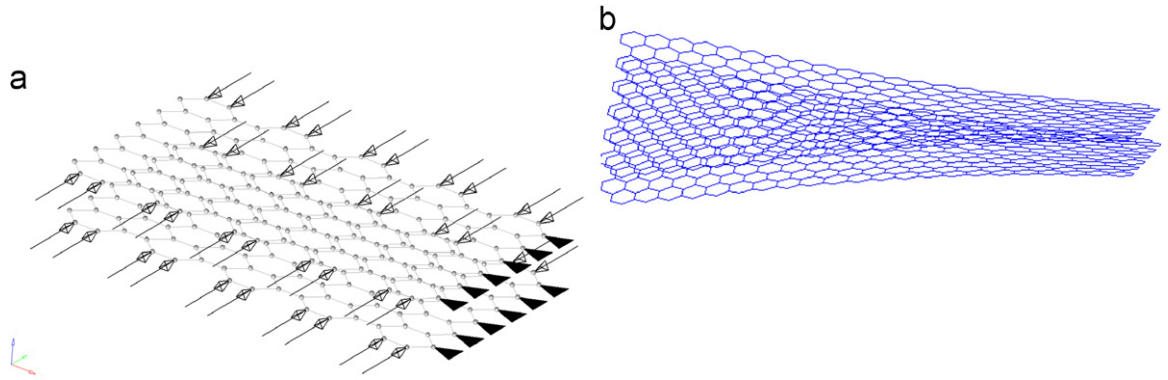

Fig. 2. Cantilever BLGS and its first buckling mode shape. The forces are prescribed at the edges to simulate buckling behavior. (a) Cantilever SLGS and (b) First buckling mode shape for cantilever SLGS.

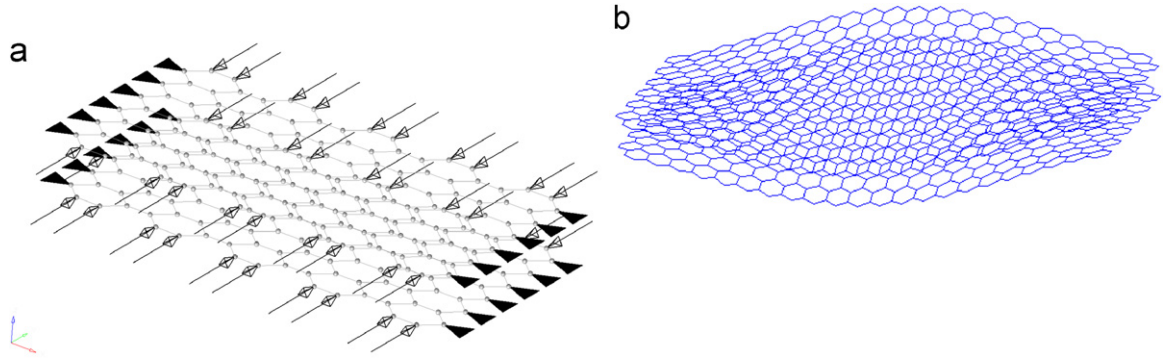

Fig. 3. Bridge BLGS and its first buckling mode shape. The forces are prescribed at the edges to simulate buckling behavior. (a) Bridge SLGS and (b) First buckling mode shape for bridge SLGS.

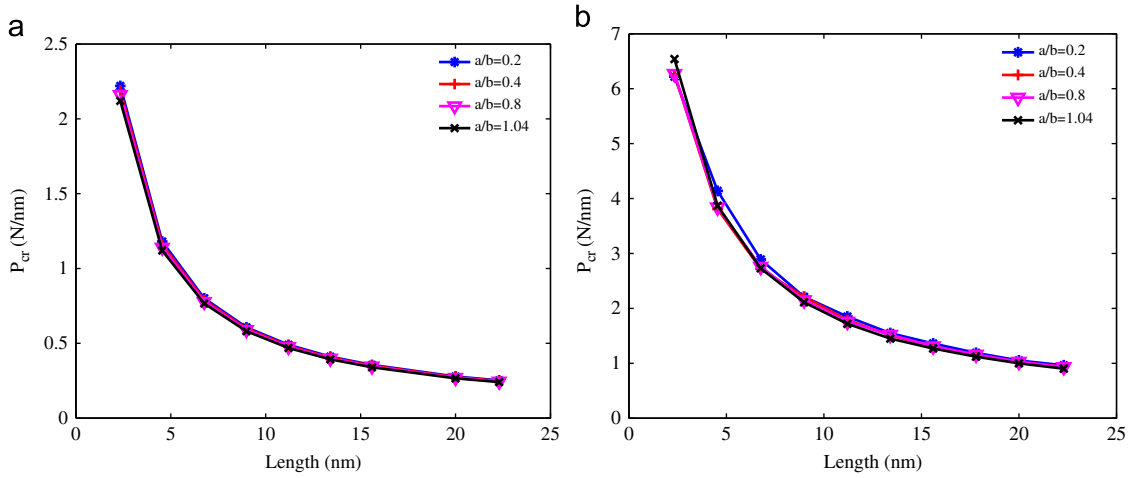

Fig. 4. Variation of buckling loads with length for SLGS at four different values of aspect ratio. The aspect ratio considered are 0.2, 0.4, 0.8 and 1.04. For cantilever sheet, the buckling load at 2.34 nm side length is 2.22 N/nm and at 22.3 nm side length is 0.25 N/nm. For bridge sheet, the buckling load at 2.34 nm side length is 6.22 N/nm and at 22.3 nm side length is 1.0 N/nm. (a) Buckling loads for cantilever SLGS. (b) Buckling loads for bridged SLGS.

edges fixed will increase the critical buckling to about three times. This trend remains same for BLGS (see Fig. 5). For SLGS models, the slope for cantilever and bridge plots is found to be identical. Whereas for BLGS models, the slope for cantilever model is found to be higher than that of bridge model. This difference occurs due to the presence of nonlinear interlayer L-J potential in BLGS.

3.3. *Dependence on number of graphene layers in the sheet*

From the above discussion, it is understood that a bilayer graphene (see Fig. 6) sheet offers stiffer response as compared to a single-layer sheet. This can be further clarified by referring to Table 1. The trend of variation of BLGS critical load with side length is found to be identical with that of SLGS. This trend confirms reduction in critical load with increase in length. However, there is a noticeable difference in slope. The slope for SLGS is found to be higher than that of BLGS. This indicates that the rate at which critical buckling load decreases with length is higher for SLGS. By referring to Table 1, we can conclude that BLGS is stiffer than SLGS. At lower side length (i.e. 3.24 nm) the bilayer structure is found to be 30 times stronger than that of single layer. At higher length (i.e. 20 nm), this factor is found to be as high as 80.

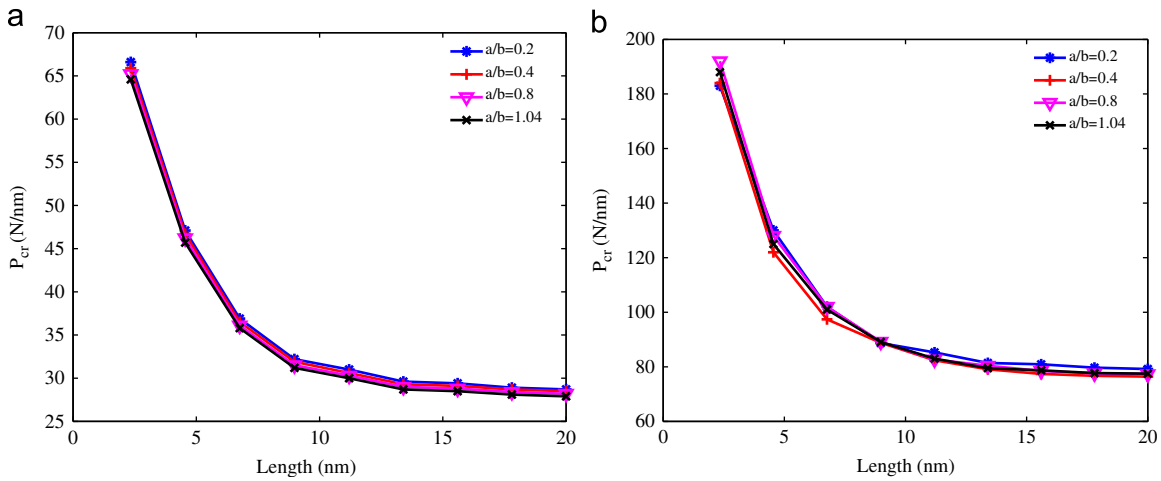

Fig. 5. Variation of buckling loads with length for BLGS at four different values of aspect ratio. The aspect ratio considered are 0.2, 0.4, 0.8 and 1.04. For cantilever sheet, the buckling load at 2.34 nm side length is 66.0 N/nm and at 22.3 nm side length is 28.0 N/nm. For bridge sheet, the buckling load at 2.34 nm side length is 183.0 N/nm and at 22.3 nm side length is 80.0 N/nm. (a) Buckling loads for cantilevered BLGS. (b) Buckling loads for bridged BLGS.

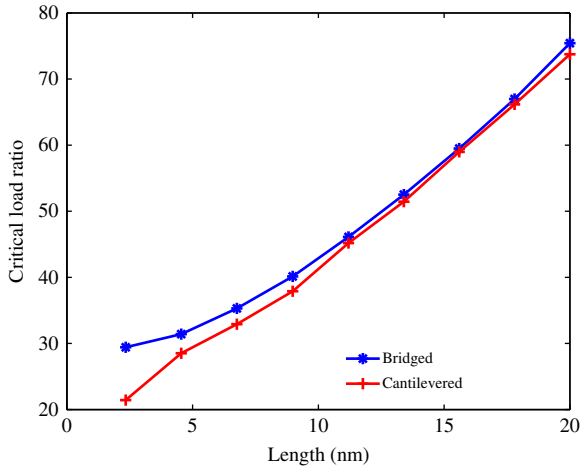

Fig. 6. The ratio of critical buckling loads between BLGS and SLGS. The length has been varied between 2.34 and 20.0 nm. Compared to SLGS, for cantilevered BLGS sheets, the buckling load increases from 21 times at 2.34 nm length to 74 times at 20.0 nm length. Similarly, for bridged sheets, the buckling load increases from 30 times at 2.34 nm length to 76 times at 20.0 nm length.

Table 1
Comparison of BLGS buckling loads against SLGS buckling loads. Graphene sheets considered here are bridged in nature. BLGS predicts about 30–80 times higher buckling strength than SLGS. Length has been varied by keeping aspect ratio 0.24.

Length (nm)	Width (nm)	P_{BLGS} (N)	P_{SLGS} (N)
2.34	9.44	183.0	6.22
4.55	18.8	130.0	4.14
6.76	28.3	100.2	2.89
8.98	37.6	88.7	2.21
11.2	46.9	85.3	1.85
13.4	56.3	81.4	1.55
15.6	65.7	80.9	1.36
17.8	75.0	79.7	1.19
20.0	84.4	79.2	1.05

This indicates that the factor increases with the side length. The inclusion of further layers will further enhance the buckling strength of the nanostructure.

4. Conclusions

The stiffness and in-plane buckling properties of single and bilayer graphene sheets are investigated using atomistic finite element approach. The C–C bonds are represented by equivalent structural beams with stretching, bending, torsional and deep shear deformation, based on the equivalence between the harmonic potential expressed in terms of Morse force-field model. This analysis confirms that, bilayer graphene sheets offer higher stiffness leading to a higher value of critical buckling load. For both single and bilayer sheets, the critical buckling load decreases with the increase in the side-length. The bucking response of graphene sheets is found to be not sensitive to the aspect ratio at a given side-length. The bridged configurations are found to be exhibiting higher critical buckling loads as compared to cantilevered configurations. The critical buckling load increases considerably with the increase in the number of graphene layers. Our results show that critical buckling loads of bilayer graphene sheets are in excess of 20 times that of single-layer graphene sheets. This implies that bilayer graphene sheets can be a superior choice for the future generation of nano-composite materials.

Acknowledgements

R.C. acknowledges the support of Royal Society through the award of Newton International Fellowship. S.A. gratefully acknowledges the support of The Royal Society of London through the Wolfson Research Merit award.

References

[1] Y. Gan, W. Chu, L. Qiao, Surface Science 539 (1–3) (2003) 120.
[2] K.S. Novoselov, A.K. Geim, S.V. Morozov, D. Jiang, Y. Zhang, S.V. Dubonos, I.V. Grigorieva, A.A. Firsov, Science 306 (2004) 5696.
[3] J.C. Meyer, A.K. Geim, M.I. Katsnelson, K.S. Novoselov, D. Obergfell, S. Roth, C. Girit, A. Zettl, Solid State Communications 143 (1–2) (2007) 101.
[4] R. Chowdhury, S. Adhikari, P. Rees, F. Scarpa, S.P. Wilks, Physical Review B 83 (4) (2011) 045401:1-8.
[5] K.I. Tserpesa, P. Papanikos, Composites Part B: Engineering 36 (2005) 1359.
[6] A.N. Pal, A. Ghosh, Applied Physics Letters 95 (8) (2009) 082105.
[7] A.N. Pal, A. Ghosh, Physical Review Letters 102 (12) (2009) 126805.
[8] J.B. Oostinga, H.B. Heersche, X. Liu, A.F. Morpurgo, L.M.K. Vandersypen, Nature Materials 7 (2008) 151.
[9] E.V. Castro, N.M.R. Peres, J.M.B. Lopes Dos Santos, F. Guinea, A.H.J. Castro Neto, Physics Conference Series 129 (2008) 012002.

[10] S.S. Gupta, R.C. Batra, Journal of Computational and Theoretical Nanoscience 7 (2010) 1546.
[11] M.M. Shokrieh, R. Rafiee, Materials and Design 31 (2010) 790.
[12] F. Scarpa, S. Adhikari, R. Chowdhury, Physics Letters A 374 (19–20) (2010) 2053.
[13] X.Q. Hea, S. Kitipornchaia, K.M. Liew, Journal of Mechanics and Physics of Solids 53 (2005) 303.
[14] S. Kitipornchaia, X.Q. Hea, K.M. Liew, Physical Review B 72 (2005) 075443.
[15] K.M. Liew, X.Q. He, S. Kitipornchai, Acta Materialia 54 (16) (2006) 4229.
[16] K. Behfar, R. Naghdabadi, Composites Science and Technology 65 (7–8) (2005) 1159.
[17] S.C. Pradhan, J.K. Phadikar, Journal of Computational and Theoretical Nanoscience 7 (2010) 1948.
[18] S.C. Pradhan, Physics Letters A 373 (2009) 4182.
[19] A. Sears, R.C. Batra, Physical Review B 73 (2006) 085410.
[20] R. Chowdhury, S. Adhikari, C.Y. Wang, F. Scarpa, Computational Materials Science 48 (4) (2010) 730.
[21] R. Ansari, S. Rouhi, Physica E 43 (2010) 58.
[22] F. Scarpa, S. Adhikari, A.S. Phani, Nanotechnology 20 (2009) 065709.
[23] T. Belytschko, S.P. Xiao, R.S. Ruoff, Physical Review B 65 (2002) 235430.
[24] K.I. Tserpes, P. Papanikos, Composites Part B 36 (2005) 468.
[25] R. Chowdhury, C.Y. Wang, S. Adhikari, Journal of Physics D: Applied Physics 43 (8) (2010) 085405.
[26] S. Adhikari, R. Chowdhury, Journal of Applied Physics 107 (12) (2010) 124322:1-8.
[27] T. Kaneko, Journal of Physics D Applied Physics 8 (1974) 1927.
[28] D. Marquardt, Journal of the Society for Industrial and Applied Mathematics 11 (2) (1963) 431.
[29] J.S. Przemienicki, Theory of Matrix Structural Analysis, McGraw-Hill, New York, 1968.
[30] L.A. Girifalco, M. Hodak, R.S. Lee, Physical Review B 62 (2001) 13104.
[31] S.P. Timoshenko, Theory of Plates and Shells, McGraw-Hill, New York, 1940.
[32] S.P. Timoshenko, J.M. Gere, Theory of Elastic Stability, McGraw-Hill, New York, 1961.